Original Article

Institution of MECHANICAL ENGINEERS

Journal of MATERIALS: DESIGN AND APPLICATIONS

Proc IMechE Part L:
J Materials: Design and Applications
2016, Vol. 230(1) 263–272

DOI: 10.1177/1464420715569289
pil.sagepub.com

SAGE

The effects of die geometry in tube channel pressing: Severe plastic deformation

MH Farshidi and M Kazeminezhad

Abstract

The effects of die geometry on the deformation behavior of aluminum 6061 alloy tube in a novel severe plastic deformation (SPD) process called tube channel pressing (TCP) were studied using the Abaqus 6.10 software. Using the optimized die geometry, 1 to 3 passes of TCP is imposed not only to validate the simulation results, but also to investigate the performance of TCP as a SPD process. The finite element method (FEM) simulation results show that the moderated plastic strain, the lower inhomogeneity in distribution of plastic strain, and the lower risk of fracture during process can be obtained using the proper die geometry. In addition, the imposed strain is a mixture of shear strain and hoop strain accompanying with little bending strain which makes it relatively different from conventional SPD processes. Experiments shows that the experimentally obtained load–displacement curve of TCP is very close to its FEM predicted counterpart which validates the FEM simulation results. Additionally, after imposing of 3 passes of TCP to 6061 alloy, the grain size of the tube is decreased from a few tens of microns to less than 1 μm while the yield strength is increased from 110 MPa to 325 MPa which show the capability of TCP as a SPD process for tubes.

Keywords

Severe plastic deformation, tube channel pressing, die design, finite element method simulation, strain and stress analysis

Date received: 14 April 2014; accepted: 30 December 2014

Introduction

Severe plastic deformation (SPD) processes have been characterized during last decades because of their capabilities in the mechanical properties improvement and the materials grain refinement.[1] As a result, different processes such as equal channel angular pressing (ECAP) for rods, high-pressure torsion (HPT) for disks, and accumulative roll bonding (ARB) for sheets are the famous ones developed for SPD of materials.[2–4]

Although, many SPD processes have been introduced for different shapes of materials,[1] the SPD of tubes has been remained less considered and few studies have been focused on it. For example, Naghasekhar et al.[5] have tried to develop ECAP for tubular elements. In this process, a close-ended tubular element is subjected to ECAP process which causes shear strain. The inner and outer angles of channel in this process are reported to be 30° and 150°, respectively. This results to the average plastic strain of about 0.3 in each pass of this process which is impressively lower than the average strain of other SPD processes. For comparison, each pass of ARB and orthogonal ECAP imposes the average strain of about 0.8 and 1.15, respectively. In addition, the tubular ECAP uses close-ended tubular element which limits the application of this process. Toth et al.[6] have developed high-pressure tube twisting (HPTT) process for SPD of tubes. In this process, the tube is subjected between a pressing mandrel inside the tube and a twisting rigid disk outside of tube which causes incidence of shear strain in tube wall. Although, this process is capable to impose relatively high strains as about 10, some problems such as the high strain inhomogeneity, the earring of tube during deformation and the limitation of the tube length restrict the application of this process. Based on the ARB process, Mohebbi and Akbarzadeh[7] developed a new SPD process for tube named accumulative spin bonding (ASB). In this process, two tubes with different diameters are inserted and bonded by a cylindrical rotating roller. The main disadvantage of this process is using tubes with

Department of Materials Science and Engineering, Sharif University of Technology, Tehran, Iran

Corresponding author:
M Kazeminezhad, Department of Materials Science and Engineering, Sharif University of Technology, Azadi Avenue, Tehran, Iran.
Email: mkazemi@sharif.edu

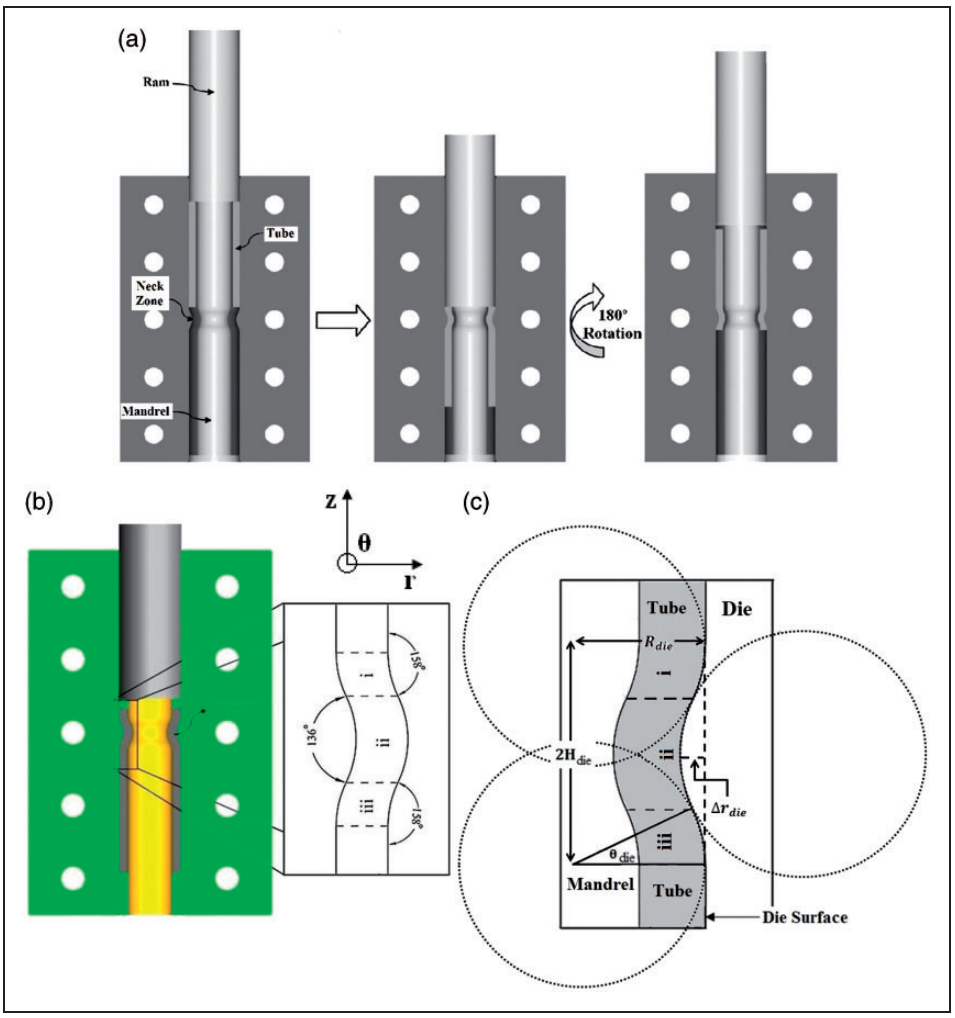

Figure 1. Principles of TCP.

Table 1. Geometrical parameters of simulated TCP dies.

Die code	R_{die}(mm)	r_{die}(mm)	RDCR	RHDC
3.75D0.75	3.75	0.75	0.29	0.058
3.75D1.5	3.75	1.5	0.29	0.115
3.75D2.2	3.75	2.2	0.29	0.17
7.5D0.75	7.5	0.75	0.58	0.058
7.5D1.5	7.5	1.5	0.58	0.115
7.5D3	7.5	3	0.58	0.23
15D0.75	15	0.75	1.15	0.058
15D1.5	15	1.5	1.15	0.115
15D3	15	3	1.15	0.23

different diameters. In addition, the distribution of strain is relatively inhomogenous in this process. To overcome the limitations of SPD of tube, a new process for SPD of tube has been recently introduced[8,9] named tube channel pressing (TCP).

As shown before, the die geometry can affect the SPD processes extensively and the improper die geometry results to different difficulties such as the strain inhomogeneity and the fracture during SPD process.[10–12] On the other hand, since TCP is relatively a new process, the effect of die geometry in this process has not yet been studied. Regarding so, the aim of this work is to study the effect of die geometry on the deformation behavior of tube during TCP.

Principles of TCP

As shown in Figure 1(a), the tube is pressed through a bottleneck region between the die and the mandrel during TCP which causes a successive decrease and increase in the tube diameter. This leads not only to impose hoop strains, but also to change of the tube wall curvature which causes shear strains.[8]

The surface of the die in the bottleneck region consists of three tangent circles as can be seen in Figure 1(b) and (c). As shown in Figure 1(c), the geometrical parameters of the die can be presented as: length of deformation zone (H_{die}), height of die convex (Δr_{die}), contact angle of circles (θ_{die}), and die

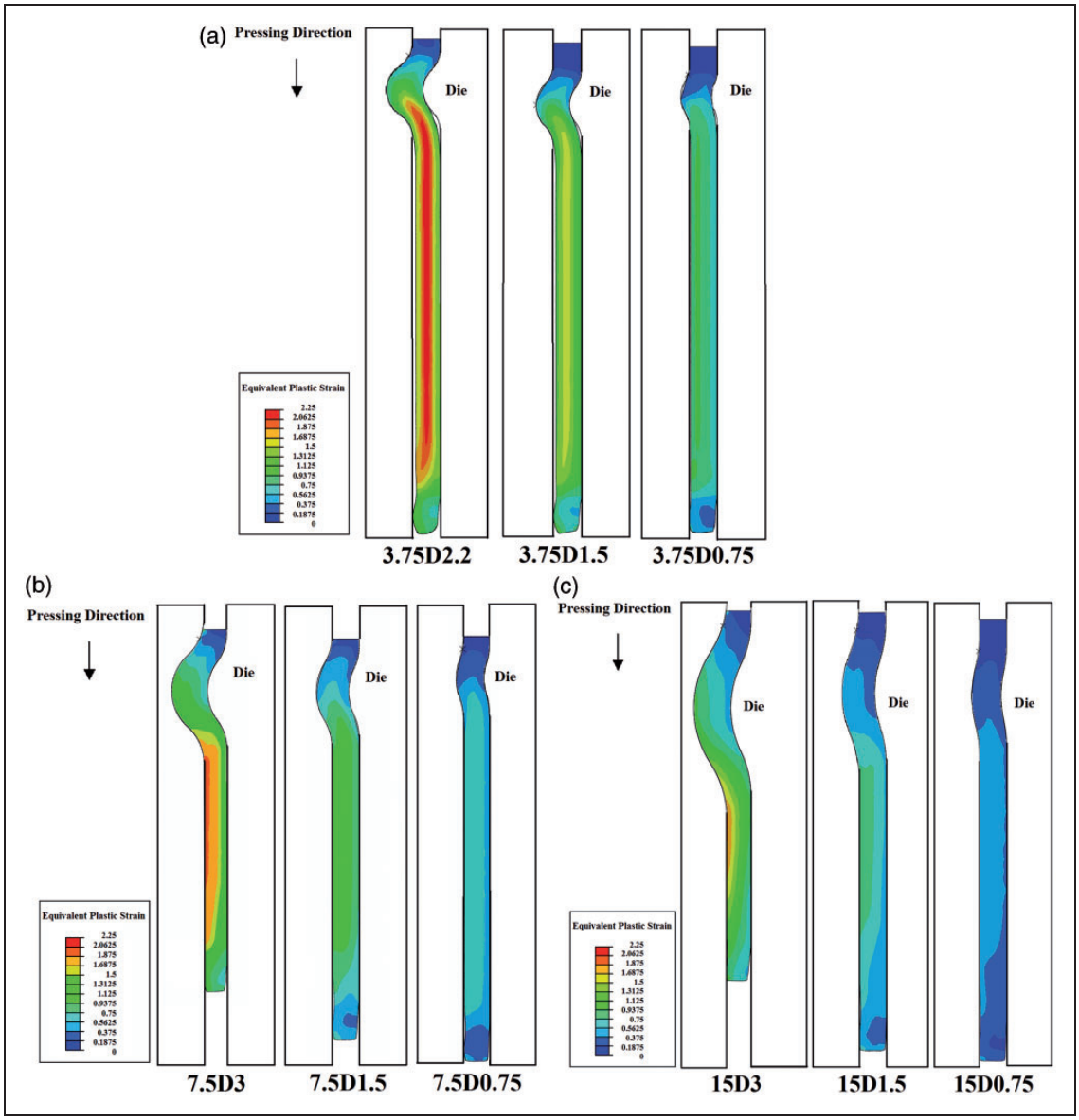

Figure 2. Distribution of plastic strain and shape of specimen using different dies: (a) dies with curvature radius of 3.75 mm; (b) dies with curvature radius of 7.5 mm; (c) dies with curvature radius of 15 mm.

curvature radius (R_{die}). Regarding so, these parameters have the following relations

$$\Delta r_{die} = 2R_{die}(1 - \cos\theta_{die}) \quad (1)$$

$$H_{die} = 2R_{die}\sin\theta_{die} \quad (2)$$

As a result, the die geometry can be defined by two independent parameters such as R_{die} and Δr_{die}. The deformation behavior of tube during TCP is also related to the dimension of tube. Thus, the effect of die geometry must be studied by dimensionless ratios such as relative die curvature radius (RDCR $= R_{die}/R_{tube}$) and relative height of die convex (RHDC $= \Delta r_{die}/R_{tube}$). Here, R_{tube} is the outer radius of tube. The mandrel geometry also affects the deformation behavior of tube during TCP which was studied previously.[9]

Procedure, experiments, and material

Deformation behaviors of tube in nine TCP dies with different geometries were simulated by Abaqus 6.10. The geometrical parameters of the studied dies are shown in Table 1. As can be seen, the RHDC and RDRC are ranged 0.058–0.23 and 0.29–1.15, respectively. The inner and outer diameters of used tube were 19 mm and 26 mm, respectively. The mandrel for each die was designed regarding the optimized mandrel design proposed previously.[8] In this mandrel design, the tube wall cross-sectional area in the middle of deformation zone was equal to its magnitude before deformation and the mandrel curvature radius was selected similar to the die curvature radius to prevent the thinning of tube during process. The material of

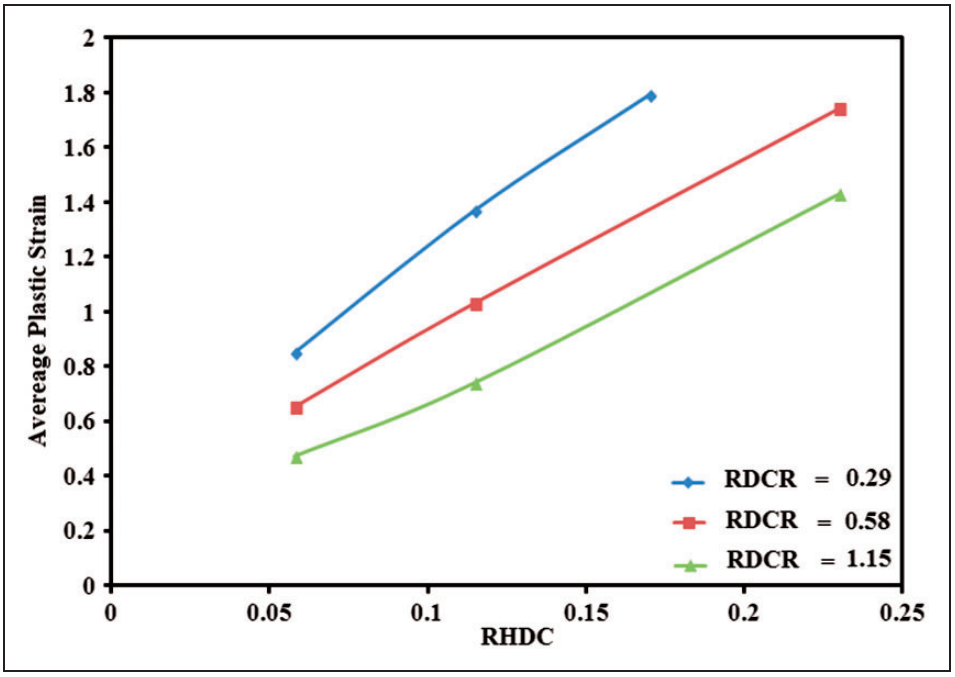

Figure 3. The plastic strain versus die geometrical parameters of TCP.
RDCR: relative die curvature radius.

tube was supposed to be solid solution treated aluminum 6061 alloy.

The applied solution for FEM simulations was "dynamic explicit" method based on Lagrangian formulation. Regarding the axial symmetry of TCP process, a 2D axi-symmetric model was applied to reduce the needed calculations. The tube was considered as deformable while other parts were considered as discrete rigid. The die and mandrel were meshed by the RAX2 one-dimensional elements. The mesh size of the die and mandrel was considered as 14 mm out of the deformation zone while it was considered as 0.5 mm in the deformation zone in order to define smooth pattern of this zone. The tube was meshed using the CAX4R two-dimensional elements. The mesh size of tube was considered 0.5×0.5 mm^2. To investigate the effect of mesh size, one simulation was carried out by halved mesh size. This simulation showed negligible difference with original simulation. For example, the maximum difference in the plastic strain was less than 5% in each point.

Concerning high strain imposed during SPD processes, stress–strain relation of the used alloy should be obtained regarding the basis of dislocation models. One of the most applied dislocation model is ETMB (Estrin, Toth, Molinari, and Brechet) model,[13] which predicts the strength of alloy considering the microstructural evolution. On the other hand, ETMB model for aluminum is identically matched to Voce relation[14] as shown before.[15] Thus, stress–strain relation of used alloy is extrapolated using Voce relation presented below

$$\sigma_f = \sigma_\infty - (\sigma_\infty - \sigma_0)\exp(-k\varepsilon_p) \tag{3}$$

where ε_p is the plastic strain, σ_f is the flow stress, σ_∞ is the saturation stress, σ_0 is the flow stress before deformation, and k is a material constant. The amounts of parameters for Voce relation were calculated by comparison of the strength of used material before and after imposing different plastic strains as presented before.[9]

Since high strain is imposed during SPD processes, the risk of fracture during process should be considered. The most probable mechanism in fracture of ductile metals such as the aluminum 6061 alloy is reported to be nucleation, coalescence, and growth of voids.[16] As a result, Ayada fracture criterion[17] can be used to predict fracture initiation during process as below

$$\int_o^{\varepsilon_f} \frac{\sigma_m}{c\sigma_f}\, d\varepsilon_p = 1 \tag{4}$$

where σ_m is the hydrostatic stress, ε_f is the fracture strain, and c is a material constant. The amount of c was calculated about 0.33 using the results of tension experiments on the as solution treated material.

In order to validate the FEM simulation results and to study the effect of TCP on materials properties, experimental studies were performed using optimum die geometry. For this purpose, solid solution treated aluminum 6061 alloy tube with chemical composition of Al–1.01 Mg–0.49Si–0.31Cu–0.24Fe–0.06Cr wt% was used. MoS_2 aerosol was used for lubrication of die, mandrel, ram, and specimen surfaces. To investigate the strengthening effect of TCP, tension test was performed on TCP processed tubes at strain rate of $5 \times 10^{-4}\,s^{-1}$ using standard specimens.[8] Microstructural studies were also carried out on

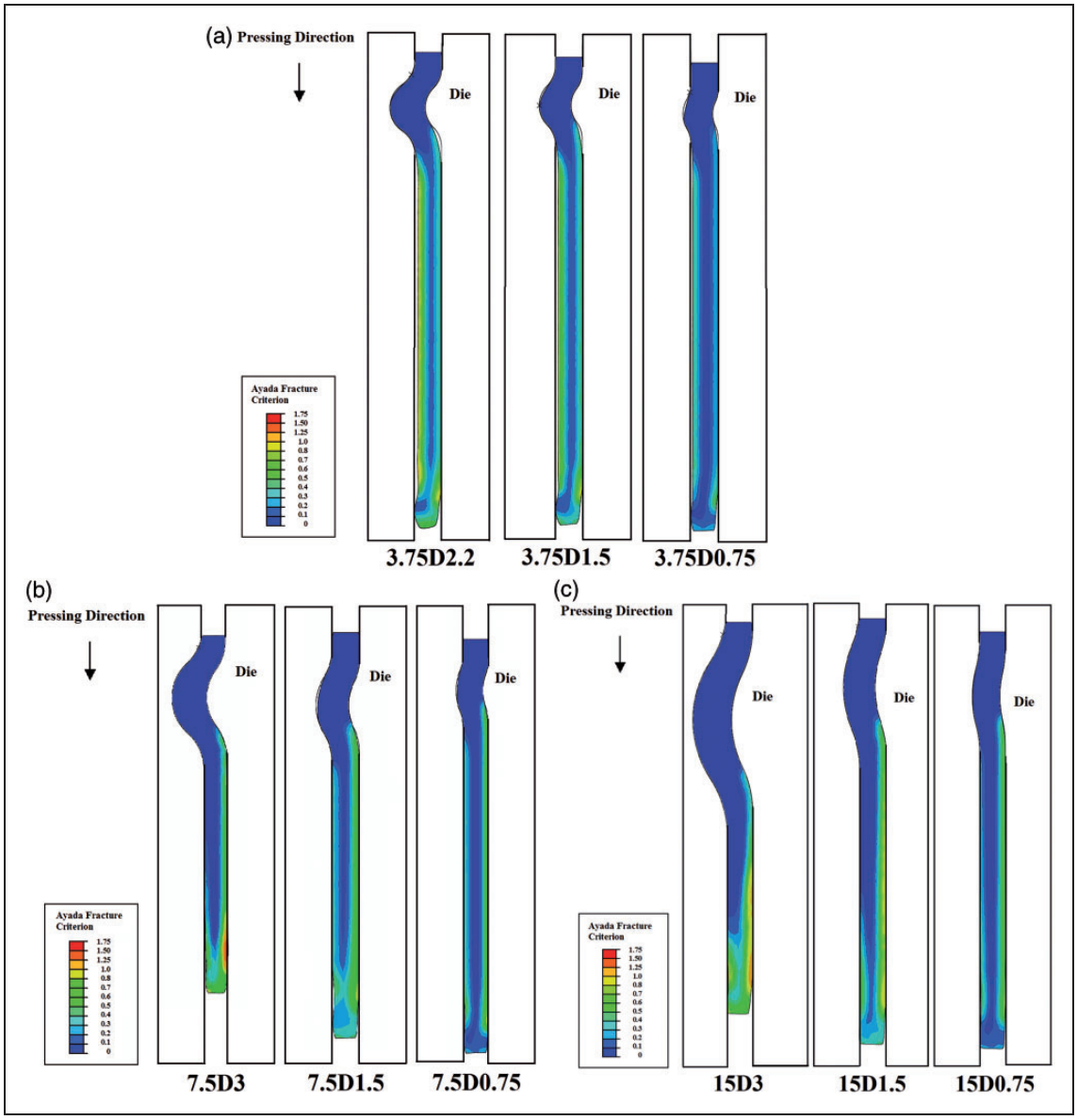

Figure 4. Distribution of Ayada fracture criterion using different dies: (a) dies with curvature radius of 3.75 mm; (b) dies with curvature radius of 7.5 mm; (c) dies with curvature radius of 15 mm.

processed tubes by optical microscope and transmission electron microscope (TEM) to investigate the effect of TCP on refinement of tube microstructure.

Results and discussion

Deformation behaviors of tube in different dies

Figure 2 shows the simulated distributions of plastic strain and the shapes of specimens using different dies. As can be seen, the higher RHDC causes the higher plastic strain and higher inhomogeneity in the distribution of plastic strain. For example, the plastic strain is more than 2 in the middle of the tube wall using the 3.75D3 die. Although, this is a remarkable strain, the distribution of strain is very inhomogenous in this die which results to decrease of strain to about 1 in the outer side of tube. Additionally, very low RDCR results to thinning of the tube wall as can be observed in 3.75D2.2 and 3.75D1.5 dies. Considering Figure 2(a) to (c), it can be inferred that the increase of RDCR in a constant RHDC results to lower plastic strain.

Figure 3 presents the average plastic strain versus die geometrical parameters. As can be seen, the average plastic strain is rapidly increased with increasing of the RHDC while it is moderately increased with decreasing of RDCR. In addition, the relation between the average plastic strain and RHDC is relatively linear. Comparatively, any decrease of RDCR to half results to an increase of about 0.2–0.5 in average plastic strain.

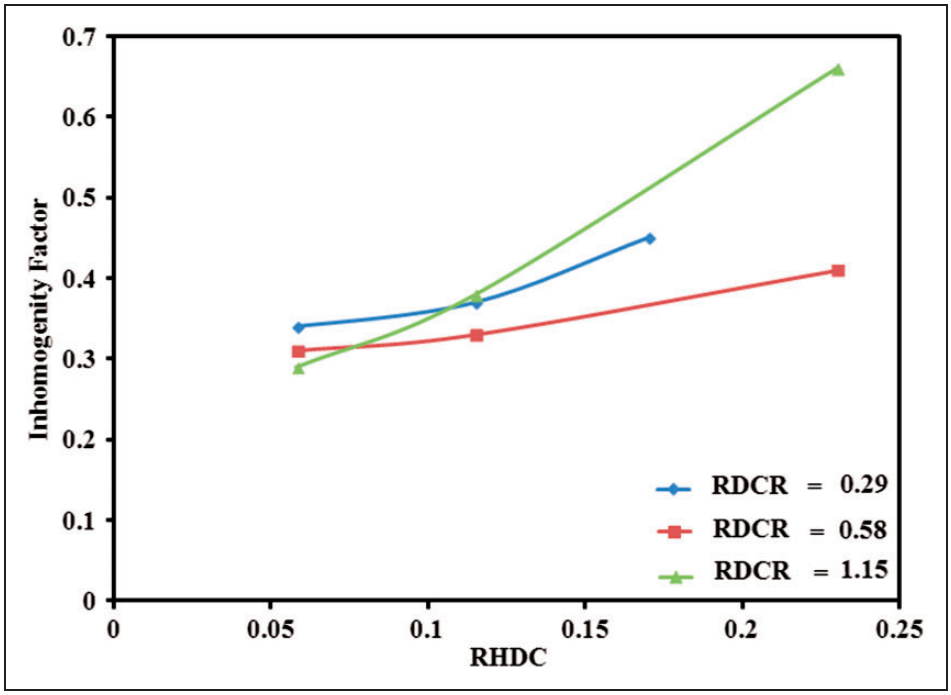

Figure 5. The inhomogeneity factor versus the geometrical parameters of TCP.
RDCR: relative die curvature radius.

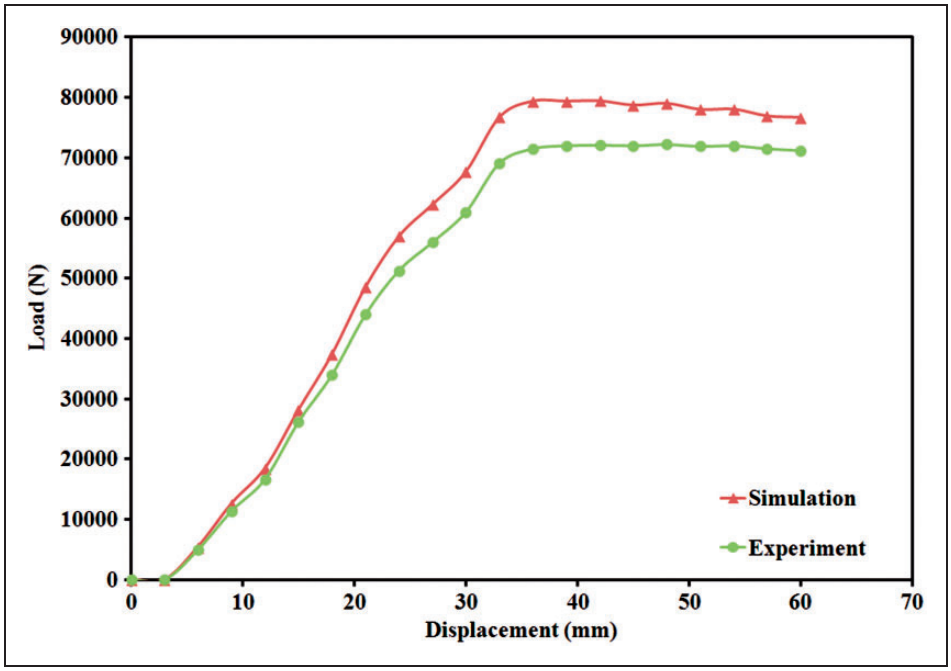

Figure 6. Comparison between simulated load-displacement curve and experimental load–displacement of TCP using 7.5D1.5 die.

Considering what told above, one may compare the effect of geometrical parameters of a die (R_{die} and Δr_{die}) with the deformation behavior of tube during TCP. In fact, each of geometrical parameter is represented by one dimensionless parameter. Therefore, the change of deformation behavior by variation of one geometrical parameter can be realized by analyzing the effect of its dimensionless counterpart on deformation behavior. For example, increase of RHDC is interpreted as increase of Δr_{die},

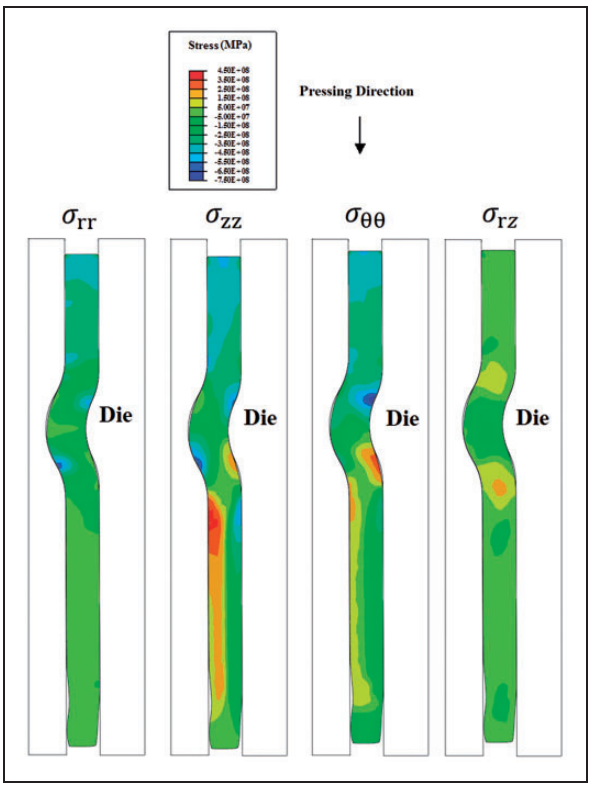

Figure 7. Distribution of stress tensor components for 7.5D1.5 die.

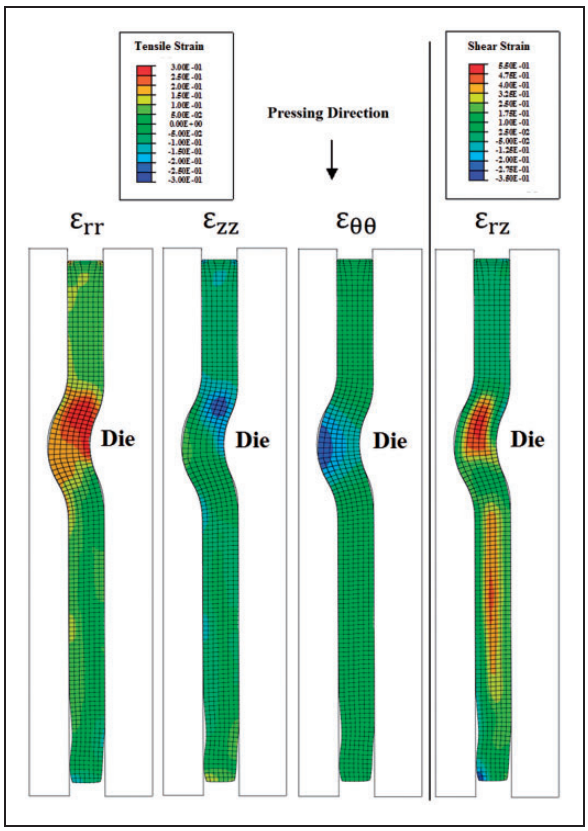

Figure 8. Distribution of strain tensor components for 7.5D1.5 die.

which results in higher variation of tube diameter during TCP. This increases the amount of imposed hoop strain which causes increase of the average plastic strain as illustrated in Figure 3. In addition, decrease of RDCR is interpreted as decrease of R_{die}. This causes impression of more severe shear strain on tube wall which results in increase of the average plastic strain as illustrated in Figure 3.

Figure 4 shows the distribution of Ayada fracture criterion in different dies. As can be seen, the higher RHDC causes higher probability of fracture during TCP. For example, the amount of Ayada fracture criterion is higher than 1 in some parts of specimens processed by 7.5D3 and 15D3 dies. Considering equation (4), the fracture can be started when the Ayada fracture criterion crosses the critical value of 1. Therefore, the fracture of specimens can be expected during processing of tube by these dies. As a result, it can be demonstrated that although the higher RHDC causes higher plastic strain, selection of very high values for RHDC is not desired due to the high risk of fracture.

Figure 5 shows the variation of inhomogeneity factor (IF) of plastic strain in different dies. Note that the IF can be obtained as

$$I.F = \frac{\varepsilon_{max} - \varepsilon_{min}}{\varepsilon_{average}} \quad (5)$$

Here, ε_{max}, ε_{min}, and $\varepsilon_{average}$ are the maximum, minimum, and average plastic strains in the tube wall, respectively. As can be seen in Figure 5, the higher RHDC causes higher IF. Additionally, utilizing the medium range of RDCR results to moderated IF while high or low value of RDCR causes increase in IF. Also, high RDCR results to rapid increase in IF versus RHDC.

The selected die geometry for SPD of tube should result to reasonable and homogenous plastic strain, low risk of fracture, and low variation of tube dimensions during process. Regarding so, one may compare the effects of RHDC with those of RDCR on the deformation behavior of tube during TCP. For example, the increase of RHDC results to a notable increase of the plastic strain. However, this can also result to the higher strain inhomogeneity and the higher risk of fracture during process. On the other hand, the decrease of RDCR results to the moderated increase of plastic strain but causes the risk of thinning of tube during process. Additionally, the minimum strain inhomogeneity is obtained in the moderated amount of RDRC. Comparing the presented results in Figure 2 with those in Figure 5, it can be inferred that the optimum die geometry can be achieved by selection of the RHDC and RDCR in ranges of 0.08–0.15 and 0.5–0.7, respectively. Thus, the 7.5D1.5 die is selected for experimental studies.

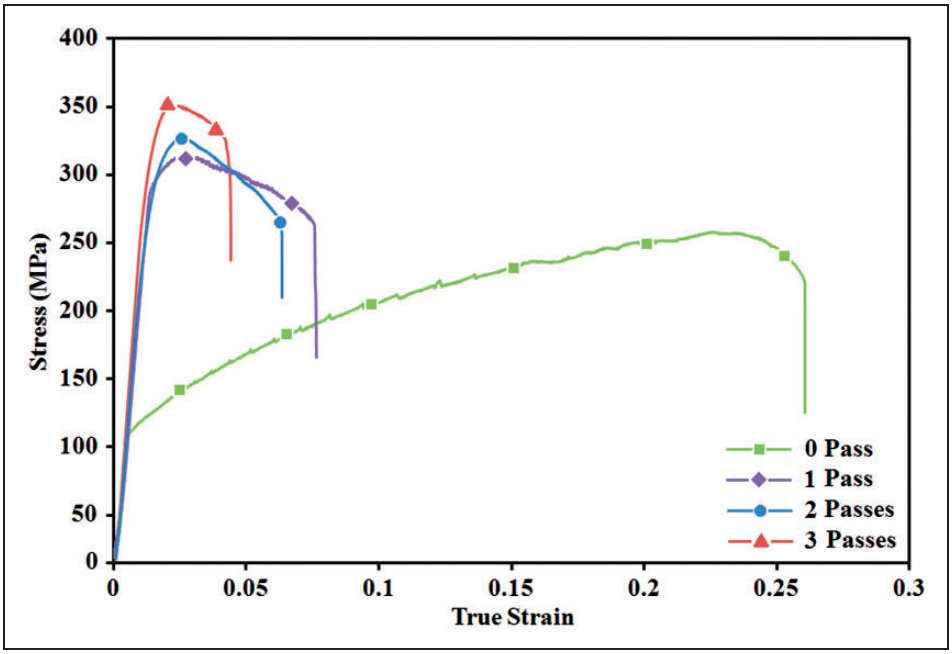

Figure 9. Tensile stress–strain curves of aluminum 6061 alloy before and after 1 to 3 passes of TCP using 7.5D1.5 die.

Simulated load–displacement curve of TCP using the 7.5D1.5 die is compared with experimental result in Figure 6. As shown here, similar trend can be seen in load–displacement curves obtained by experiment and simulation. As an illustration, the load is negligible just after start of ram displacement since edge of the tube wall bends easily and continues its way to the empty bottleneck region. The amount of friction is also negligible due to clearance of die/mandrel and tube. Therefore, a notable increase of load starts only when the bottleneck zone is filled by tube and the tube wall becomes thicker which causes the increase of deformation load and frictional load, respectively. After a rapid increase, the load reaches to a plateau which represents the steady-state step of process. Considering these similarities between results of simulation and experiment, it can be inferred that the applied simulation is a valid approach for prediction of tube deformation behavior during TCP.

Strain and stress condition in TCP

Figure 7 shows the simulated distribution of stress tensor components in the specimen during TCP. As can be seen, the amount of shear stress (σ_{rz}) is drastically shifted in the deformation zone which shows the incidence of shear strain in this zone. On the other hand, extensive variation of σ_{zz} in the veer points of tube wall in deformation zone represents appearance of the limited bending deformation regions. In addition, a remarkable amount of stress can be traced after deformation which illustrates generation of residual stress in tube during processing by TCP.

Figure 8 shows the simulated distribution of strain tensor components in the specimen during TCP. As shown here, the shear strain (ε_{rz}) is drastically increased in the entrance region of deformation zone, which represents the incidence of the shear strain in the TCP process mentioned before. The shear strain is mainly concentrated in the middle of the tube wall thickness and its amount is very low inside or outside of the tube. Negative amounts of hoop strain ($\varepsilon_{\theta\theta}$) can be also observed in the middle of deformation zone. The absolute value of $\varepsilon_{\theta\theta}$ is impressively higher in the internal side of tube wall which represents higher hoop strain inside the tube. Additionally, the absolute amount of ε_{zz} is highly shifted on the veer points of tube wall which represents the incidence of bending strain in these points. These veer points are located inside or outside of the tube near the tube surfaces as can be seen in Figures 7 and 8. The mesh distortion near these surfaces also shows the limited bending strain in these regions. Considering these results, it can be inferred that the plastic strain imposed by TCP is a mixture of the shear strain, hoop strain and limited bending strain. This makes the TCP differs from other SPD processes where the imposed strain is usually pure. As an illustration, in the ECAP and the HPT, the mode of imposed strain is pure shear.

Capabilities of TCP as a SPD process

Figure 9 compares the results of tension test for specimens processed by 0 to 3 passes of TCP. Note that the TCP process is carried out using 7.5D1.5 die which imposes average plastic strain of about 1 in each pass. As shown here, TCP causes a notable increase in strength. For example, the yield strength

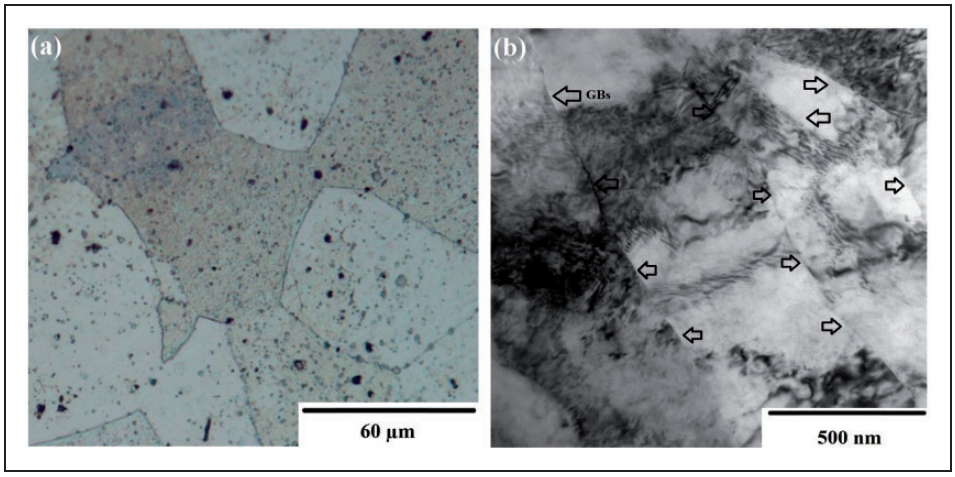

Figure 10. Microstructure of aluminum 6061 alloy: (a) before TCP; (b) after 3 passes of TCP. Note that arrows indicate grain boundaries in Figure 10(b).

of 3 passes TCPed specimen is increased to 325 MPa compared with 110 MPa before imposing TCP process. Similarly, increasing the yield strength of aluminum 6061 alloy to about 350 MPa was reported after imposing equivalent strain of about 4 using ARB and ECAP.[18,19] Thus, the capability of TCP in increasing of strength is comparable with other SPD processes such as ARB and ECAP.

Figure 10(a) presents the microstructure of tube before TCP. As can be seen, the size of grains before TCP was in range of a few tens of micrometer. Figure 10(b) shows the microstructure of tube after imposing 3 passes of TCP. As shown here, the size of grains is decreased to less than 1 μm after 3 passes of TCP. This illustrates that a notable grain refinement can be obtained by using of TCP. This is also comparable with the grain size of 0.5 μm after imposing equivalent strain of about 4 to aluminum 6061 alloy using ECAP and HPT processes as reported earlier.[20,21]

Conclusions

Considering the results of this work, it can be concluded that:

1. In order to obtain the moderated plastic strain and prevent the increase of strain inhomogeneity, the thinning of tube wall and the risk of fracture, the RDCR and RHDC of TCP process should be selected as 0.5–0.7 and 0.08–0.15, respectively.
2. Plastic strain imposed by TCP is a mixture of the shear strain and the hoop strain accompanying with limited bending strain. This makes the TCP differs from conventional SPD processes where the strain is pure.
3. The capability of TCP in grain refinement and mechanical properties improvement of materials is comparable with other SPD processes such as the ARB, ECAP, and HPT.

Acknowledgements

The authors wish to thank the research board of Sharif University of Technology for the provision of the research facilities used in this work. The authors also wish to thank Prof. Hiroyuki Miyamoto and Doshisha University for the provision of TEM facilities.

Funding

This research received no specific grant from any funding agency in the public, commercial, or not-for-profit sectors.

References

1. Estrin Y and Vinogradov A. Extreme grain refinement by severe plastic deformation: A wealth of challenging science. *Acta Mater* 2013; 61: 782–817.
2. Segal VM, Rereznikov VI, Drobyshebskiy AE, et al. Plastic working of metals by simple shear. *Russ Metall* 1981; 1: 99–105.
3. Valiev RZ, Krasilnikov NA and Tsenev NK. Plastic deformation of alloys with submicron-grained structure. *Mater Sci Eng A* 1991; 137: 35–40.
4. Tsuji N, Saito Y, Utsunomiya H, et al. Ultrafine grained bulk steel produced by Accumulative Roll-Bonding (ARB) process. *Script Mater* 1999; 40: 795–800.
5. Nagasekhar AV, Chakkingal U and Venugopal P. Candidature of equal channel angular pressing for processing of tubular commercial purity-titanium. *J Mater Process Technol* 2006; 173: 53–60.
6. Toth LS, Arzaghi M, Fundenberger JJ, et al. Severe plastic deformation of metals by high-pressure tube twisting. *Script Mater* 2009; 60: 175–177.
7. Mohebbi MS and Akbarzadeh A. Accumulative spin-bonding (ASB) as a novel SPD process for fabrication of nanostructured tubes. *Mater Sci Eng A* 2010; 528: 180–188.
8. Zangiabadi A and Kazeminezhad M. Development of a novel severe plastic deformation method for tubular materials: Tube channel pressing. *Mater Sci Eng A* 2011; 528: 5066–5072.

9. Farshidi MH and Kazeminezhad M. Deformation behavior of 6061 aluminum alloy through tube channel pressing: Severe plastic deformation. *J Mater Eng Perform* 2012; 21: 2099–2105.
10. Rosochowski A and Olejnik L. Finite element simulation of severe plastic deformation processes. *Proc IMechE, Part L: J Materials: Design Applications* 2007; 221: 187–196.
11. Deng G, Lu C, Su L, et al. Influence of outer corner angle (OCA) on the plastic deformation, and texture evolution in equal channel angular pressing. *Comput Mater Sci* 2014; 81: 79–88.
12. Luri R and Luis Perez CJ. Analysis and modelling by finite element method of the equal channel angular extrusion pressure. *Proc IMechE, Part B: J Engineering Manufacture* 2010; 224: 925–935.
13. Estrin Y, Toth LS, Molinari A, et al. A dislocation-based model for all hardening stages in large strain deformation. *Acta Mater* 1998; 46: 5509–5522.
14. Voce E. A practical strain-hardening function. *Metallurgica* 1955; 51: 219–226.
15. Kazeminezhad M and Hosseini E. Modeling of induced empirical constitutive relations on materials with FCC, BCC, and HCP crystalline structures: severe plastic deformation. *Int J Adv Manuf Technol* 2010; 47: 1033–1039.
16. Lassance D, Fabregue D, Delannay F, et al. Micromechanics of room and high temperature fracture in 6xxx Al alloys. *Prog Mater Sci* 2007; 52: 62–129.
17. Li H, Fu MW, Lu J, et al. Ductile fracture: Experiments and computations. *Int J Plasticity* 2011; 27: 147–180.
18. Rezaei MR, Toroghinejad MR and Ashrafizadeh F. Production of nano-grained structure in 6061 aluminum alloy strip by accumulative roll bonding. *Mater Sci Eng A* 2011; 529: 442–446.
19. Murashkin MY, Bobruk EV, Kilmametov AR, et al. Structure and mechanical properties of aluminum alloy 6061 subjected to equal-channel angular pressing in parallel channels. *Strength Plasticity* 2009; 108: 439–447.
20. Kim WJ, Sa YK, Kim HK, et al. Plastic forming of the equal-channel angular pressing processed 6061 aluminum alloy. *Mater Sci Eng A* 2008; 487: 360–368.
21. Loucif A, Figueiredo RB, Baudin T, et al. Microstructural evolution in an Al-6061 alloy processed by high-pressure torsion. *Mater Sci Eng A* 2010; 527: 4864–4869.